JGR Space Physics

RESEARCH ARTICLE
10.1029/2019JA026533

A Modeling Study of the Responses of Mesosphere and Lower Thermosphere Winds to Geomagnetic Storms at Middle Latitudes

Jingyuan Li[1,2], Wenbin Wang[2], Jianyong Lu[1], Jia Yue[3], Alan G. Burns[2], Tao Yuan[4], Xuetao Chen[5], and Wenjun Dong[6]

[1]Institute of Space Weather, College of Math and Statistics, Nanjing University of Information Science and Technology, Nanjing, China, [2]High Altitude Observatory, National Center for Atmospheric Research, Boulder, CO, USA, [3]Atmospheric and Planetary Sciences, Hampton University, Hampton, VA, USA, [4]Center for Atmospheric and Space Sciences, Utah State University, Logan, UT, USA, [5]CAS Key Laboratory of Geospace Environment, School of Earth and Space Sciences, University of Science and Technology of China, Hefei, China, [6]School of Electronic Information, Wuhan University, Wuhan, China

Abstract Thermosphere Ionosphere Mesosphere Electrodynamics General Circulation Model (TIMEGCM) simulations are diagnostically analyzed to investigate the causes of mesosphere and lower thermosphere (MLT) wind changes at middle latitudes during the 17 April 2002 storm. In the early phase of the storm, middle-latitude upper thermospheric wind changes are greater and occur earlier than MLT wind changes. The horizontal wind changes cause downward vertical wind changes, which are transmitted to the MLT region. Adiabatic heating and heat advection associated with downward vertical winds cause MLT temperature increases. The pressure gradient produced by these temperature changes and the Coriolis force then drive strong equatorward meridional wind changes at night, which expand toward lower latitudes. Momentum advection is minor. As the storm evolves, the enhanced MLT temperatures produce upward vertical winds. These upward winds then lead to a decreased temperature, which alters the MLT horizontal wind pattern and causes poleward wind disturbances at higher latitudes.

Plain Language Summary In a recent work, we found that in the mesosphere and lower thermosphere (MLT) region at middle latitudes, adiabatic heating/cooling and vertical heat advection, both associated with vertical wind changes, are the dominant processes that determine the temperature responses to storms. However, the cause of MLT vertical wind changes during storms has not been elucidated. Thus, there is a compelling need to understand how and why the wind changes during storms in the MLT region. Here we address this question by exploring theoretically the processes that determine the MLT wind response to storms at middle latitudes. During the early phase of the storm, the middle-latitude upper thermospheric wind changes are greater and occur earlier than those in the MLT region. The horizontal wind changes cause vertical wind changes, which are transmitted to the MLT region. The pressure gradient produced by the temperature changes associated with vertical wind changes and the Coriolis force are the dominant processes that drive storm time MLT wind changes at middle latitudes. Momentum advection is minor. As the storms evolve, the enhanced temperatures produce upward vertical winds. The upward vertical winds then lead to a depleted temperature, which consequently alters the MLT horizontal wind pattern.

Key Points:

- Pressure gradient produced by temperature changes and the Coriolis force drive the storm-time MLT wind changes at middle latitudes
- Downward vertical winds from the upper thermosphere enhance MLT temperatures, which drive equatorward winds in the storm early phase
- As storms progress, enhanced MLT temperatures create a divergent flow at middle latitude, making disturbance winds poleward and upward

Correspondence to:
J. Lu,
jylu@nuist.edu.cn

Citation:
Li, J., Wang, W., Lu, J., Yue, J., Burns, A. G., Yuan, T., et al. (2019). A modeling study of the responses of mesosphere and lower thermosphere winds to geomagnetic storms at middle latitudes. *Journal of Geophysical Research: Space Physics*, *124*, 3666–3680. https://doi.org/10.1029/2019JA026533

Received 25 JAN 2019
Accepted 22 MAR 2019
Accepted article online 24 APR 2019
Published online 15 MAY 2019

1. Introduction

Neutral winds are an important component of the coupled mesosphere-thermosphere-ionosphere system. Wind observations over the past decades have shown large-scale storm-time wind variations (e.g., McCormac et al., 1987). During geomagnetic storms, in the upper thermosphere, the greatly enhanced high-latitude energy and momentum inputs lead to strong Joule heating and ion drag, which, in turn, change the neutral temperature and global circulation. The storm-time meridional disturbance winds are mostly equatorward with disturbance velocities of ~500–800 m/s at high latitudes (Babcock & Evans, 1979; Emery et al., 1999; Richmond & Lu, 2000; Fuller-Rowell et al., 2002; Gardner & Schunk, 2010). Ion drag and pressure gradient force are the primary drivers for the high-latitude meridional wind changes in the *E* and *F* regions (e.g., Killen & Roble, 1986; Richmond et al., 2003). Storm-time high-latitude

meridional wind perturbations can quickly propagate to lower latitudes in the upper thermosphere. This propagation of wind perturbations, however, is mostly restricted to the nightside, especially during the early phase of the storm (Fuller-Rowell et al., 2002; Haaser et al., 2013).

Although we understand the general features of the upper thermosphere wind and temperature changes during storms, their response to storms in the mesosphere and lower thermosphere (MLT) region is not well understood. In the MLT region at middle latitudes, both ground- and space-based observations, although very limited, have shown that meridional winds also vary during storms. Hook (1970) found that the storm-time meridional perturbations are equatorward at middle latitudes in the altitude range of 75–110 km. Ma et al. (2001) demonstrated that MLT winds turn from poleward to equatorward and have an eastward enhancement at middle latitudes during the storms. Goncharenko et al. (2004) showed that the meridional wind differences between quiet and storm time are equatorward at altitudes between 100 and 110 km in the middle latitudes. The direction of the zonal winds is reversed from westward to eastward and with changes in the speed of an order of 100–250 m/s. The storm-time wind disturbance penetrates down to the lowest altitude of 100 km. Conversely, Fahrutdinova et al. (2001) found that storm-time MLT (80–105 km) meridional wind variations are poleward with a perturbation velocity of ~10 m/s, which even can reverse the direction of the meridional prevailing winds in all seasons. They also showed that changes in the zonal prevailing winds under disturbed magnetic conditions can reach 50% in the MLT region. Mazaudier and Bernard (1985) showed that the changes of the direction of MLT meridional winds during storms vary with altitudes.

However, Singer et al. (1994) found there are no significant changes in the MLT meridional winds at middle latitudes. In the zonal direction, there are storm-time enhanced westward winds at middle latitudes but an eastward wind enhancement at higher latitudes. Salah and Goncharenko (2001) showed that when the storm activity is moderate ($Kp < 6$), there is no strong evidence for a response in the lower thermosphere winds. However, for intense storms ($Kp > 6$), the meridional and zonal wind perturbations are greatly enhanced. The changes in the meridional winds are in different directions at different local times. The magnitude of the enhanced zonal winds and their duration depends on the intensity and duration of the storm. Emmert et al. (2002) also found that the direction of meridional wind changes with local time. The perturbation magnitude can reach up to ~50 m/s in the MLT region at ~100-km altitude. The zonal disturbance winds are mostly westward with largest magnitudes above ~150 km, and the height variation of the zonal winds is seasonally dependent. Fesen (1997) demonstrated that the meridional and perturbations caused by storms could penetrate down to lower altitudes (~100 km), which are seasonally and local-time dependent. Therefore, the observed MLT wind responses to the storms at middle latitudes are still inconclusive, sometimes contradictory, and lack of a global perspective.

A number of physical processes have been proposed to explain the storm-time MLT wind disturbances at middle latitudes. Fuller-Rowell (1995) suggested that advection may play an additional role in transporting the wind disturbances from high to lower latitudes in the lower thermosphere. Nozawa and Brekke (1995) demonstrated that only part of the E region disturbance neutral winds can be explained by ion drag. Many researchers suggested that the storm-time wind patterns are primarily controlled by pressure gradients associated with high-latitude Joule heating, the Coriolis force, and ion drag (e.g., Emmert et al., 2001, 2002, 2004, 2008; Forbes & Roble, 1990; Hagan & Sipler, 1991). However, due to limited observations and the complex processes at work (including the nonlinearly coupled electrodynamics, dynamics, thermodynamics, and chemistry in the region), the complex physical mechanisms that produce storm-time MLT neutral wind changes at middle latitudes have not been well understood.

Li et al. (2018) carried out first-principles simulations of MLT neutral temperature (T_n) response at middle latitudes using the Thermosphere Ionosphere Mesosphere Electrodynamics General Circulation Model (TIMEGCM). They showed that the simulated MLT temperature changes similar to the lidar observations (40°N, 105°W) at this place (Yuan et al., 2015). They found through diagnostic analysis of model outputs that storm-time MLT T_n changes at middle latitudes are produced mainly by adiabatic heating/cooling and heat advection associated with vertical wind changes. However, the cause of the vertical wind changes during storms has not been elucidated in that work. There is a compelling need to understand how and why vertical winds, as well as horizontal winds, change during storms in the MLT region. This paper aims to address this question by exploring theoretically the processes that determine the MLT wind response to storms at middle

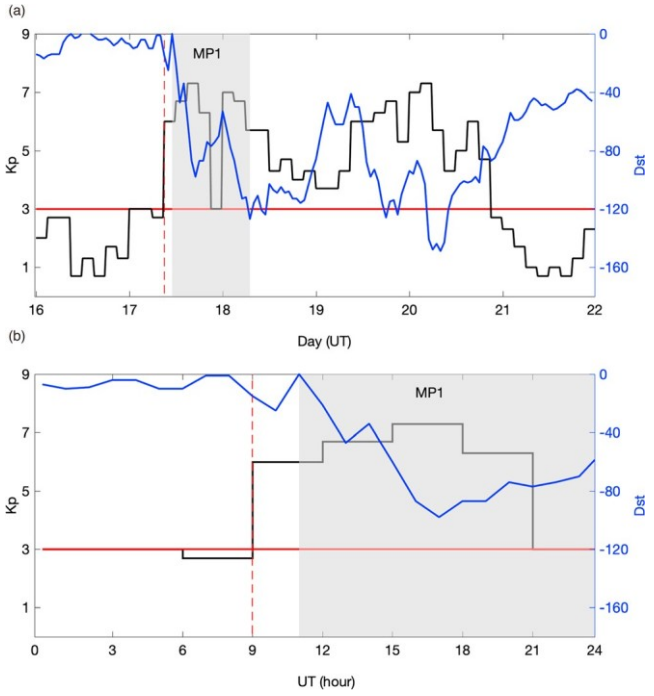

Figure 1. Variations of 3-hr *Kp* (black line) and hourly *Dst* (blue line): (a) between 16 April and 23 April and (b) between 00:00–24:00 UT on 17 April 2002: the black solid line shows the real *Kp* during the storm, and the red line is a constant *Kp* value of 3.0 for nondisturbed conditions. The red dashed lines indicate the storm onset time. The grey area indicates the first main phase (MP1) of the storm.

latitudes, which has not been done before. This is achieved by diagnostically analyzing TIMEGCM outputs of the 17 April 2002 storm, the same storm that was studied in Li et al. (2018).

2. Model Simulations

The TIMEGCM has a resolution of 2.5° × 2.5° in geographic latitude and longitude and a vertical resolution of 1/4 scale height. It is a three-dimensional global model that self-consistently simulates circulation, dynamics, photoionization, electrodynamics, chemistry, and composition of the Earth's middle and upper atmosphere (Roble & Ridley, 1994). The Heelis model (Heelis et al., 1982) is used to specify the high-latitude ion convection pattern, which is driven by the 3-hr *Kp* index. The GSWM (Hagan & Forbes, 2002, 2003), including both migrating and nonmigrating diurnal and semidiurnal, is used to specify lower atmospheric tides at the model lower boundary.

TIMEGCM simulations are diagnostically analyzed to investigate the possible physical processes that cause storm-time MLT wind changes. Two TIMEGCM runs were performed: one was driven by a constant *Kp* value of 3.0 for geomagnetically nondisturbed conditions (red lines in Figure 1) and the other by the true geophysical conditions (black lines in Figure 1). The grey area indicates the first storm main phase (MP1). The end of grey area is the beginning of the recovery phase. We are interested in the first storm main phase. The second main phase occurred at ~09:00 UT on 19 April, during the recovery phase of the first storm. The second main phase will not be the focus of the current study. Other than these different *Kp* conditions, the two runs used exactly the same initial conditions at 00:00 UT on 17 April, as well as the same other model driving parameters (such as $F_{10.7}$ and lower atmospheric tides). The model was run for 20 days with a constant *Kp* of 3 until 00:00 UT on 17 April so that the model approached a model state for a constant magnetic activity condition (*Kp* = 3) but was consistent with solar radiation and seasonal conditions before the storm. Therefore, the differences between the results of these two runs are assumed to be the storm effects on the MLT.

The meridional and zonal momentum equations are defined as follows:

$$\frac{\partial V_n}{\partial t} = \frac{ge^{z}}{p_0}\frac{\partial}{\partial Z}\left(\mu\frac{\partial V_n}{H\partial Z}\right) - f^{\mathrm{cor}}U_n + \lambda_{yy}(V_i - V_n) + \lambda_{yx}(U_i - U_n) - \vec{V}_n\cdot\nabla V_n + \frac{U_nU_n}{R_{\mathrm{E}}}\tan\lambda - \frac{1}{R_{\mathrm{E}}}\frac{\partial\Phi}{\partial\lambda} - W_n\frac{\partial U_n}{\partial Z} \quad (1)$$

$$\frac{\partial U_n}{\partial t} = \frac{ge^{z}}{p_0}\frac{\partial}{\partial Z}\left(\mu\frac{\partial U_n}{H\partial Z}\right) + f^{\mathrm{cor}}V_n + \lambda_{xx}(V_i - V_n) + \lambda_{xy}(U_i - U_n) - \vec{V}_n\cdot\nabla U_n + \frac{U_nV_n}{R_{\mathrm{E}}}\tan\lambda - \frac{1}{R_{\mathrm{E}}\cos\lambda}\frac{\partial\Phi}{\partial\phi} - W\frac{\partial U_n}{\partial Z} \quad (2)$$

where t is the time, λ is the latitude, ϕ is the longitude, g is the gravitational acceleration, p_0 is the reference pressure, μ is the viscosity coefficient, H is the pressure scale height, f^{cor} is the Coriolis parameter, λ_{yx} and λ_{yy} are the ion drag coefficients, V_n and V_i are the neutral and ion meridional velocities, U_n and U_i are the neutral and ion zonal velocities, $\vec{V}_n$ is the horizontal wind, R_{E} is the Earth's radius, Φ is the pressure, and W is the vertical wind, respectively. The terms (meridional) on the right side are the vertical viscosity ($\frac{ge^{z}}{p_0}\frac{\partial}{\partial Z}\left(\mu\frac{\partial V_n}{H\partial Z}\right)$), Coriolis force ($f^{\mathrm{cor}}U_n$), ion drag force ($\lambda_{yy}(V_i - V_n) + \lambda_{yx}(U_i - U_n)$), horizontal advection ($\vec{V}_n\cdot\nabla V_n$), centrifugal force ($\frac{U_nU_n}{R_{\mathrm{E}}}\tan\lambda$), pressure gradient force ($\frac{1}{R_{\mathrm{E}}}\frac{\partial\Phi}{\partial\lambda}$), and vertical advection ($W\frac{\partial V_n}{\partial Z}$), respectively. The zonal terms are similar to those of meridional terms. If the atmosphere behaved exactly as the model runs, then by diagnostically analyzing the relative importance of each term from those two runs, we can understand the main physical processes that cause the storm-time wind variations.

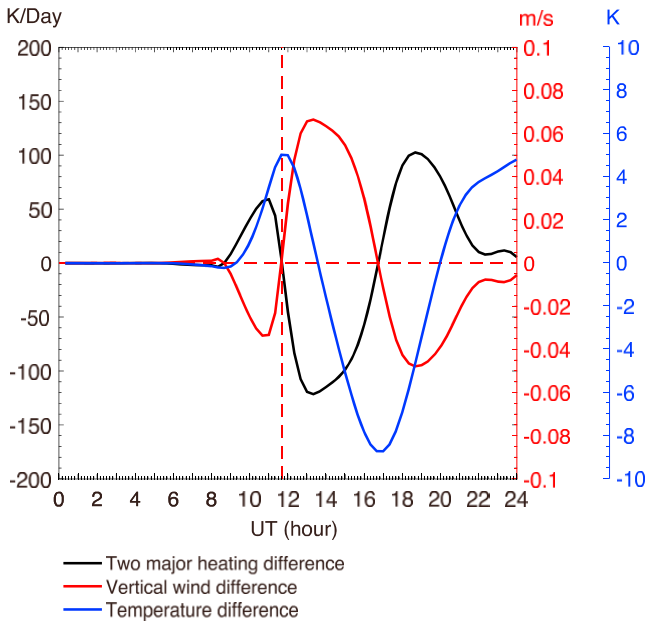

Figure 2. Differences between TIMEGCM simulations driven by real *Kp* and by a constant *Kp* value of 3.0 of (black) two major heating terms associated with vertical winds (adiabatic heating + vertical heat advection), (red) vertical winds, and (blue) neutral temperature on 17/04/2002 at 105 km and at the location of 40°N, 105°W.

3. Results

Li et al. (2018) suggested that the storm-time temperature changes at middle latitudes simulated by the TIMEGCM are similar to the observations during the 17 April 2002 storm. They demonstrated that adiabatic heating/cooling and vertical heat advection, both associated with changes in vertical winds, are the dominant processes at middle latitudes to produce the simulated storm-time MLT temperature changes. Other heating term differences are very small, such as those of Joule heating, radiative cooling, and horizontal advection, when compared with these two. Since the MLT T_n changes are closely coupled with the global three dimensional circulation changes and the TIMEGCM captured the nature and cause of MLT temperature changes, the modeled storm-time wind changes should also reasonably reflect the wind responses to storms. Thus, a diagnostic analysis of model outputs can provide a plausible approach to elucidate the physical mechanisms that drive the storm-time MLT wind changes at middle latitudes.

To further illustrate MLT T_n changes and their relationship with vertical wind and heating term changes at middle latitudes, Figure 2 shows the differences between TIMEGCM simulations driven by real *Kp* and by a constant *Kp* value of 3.0 of the total heating of adiabatic heating/cooling and vertical advection processes (black), vertical winds (red), and neutral temperature (blue) on 17 April 2002 at 105 km and at the location of 40°N, 105°W. There is a strong negative correlation between the total heating differences and vertical wind differences. It shows that a change of vertical wind speed of ~0.03 m/s can cause a change in adiabatic heating or cooling and vertical heat advection of 60 K/day (2.5 K/hr), which can lead to a temperature change of about 5 K at the beginning of the storm from 9:00 UT to 12:00 UT. The changes in vertical winds are sufficient to produce the simulated T_n changes (Li et al., 2018). Note that the peaks of T_n changes occur when vertical wind and heating terms cross the zero value points and that T_n changes lag behind the changes of vertical winds and their associated heating. This means that T_n differences increase when vertical wind differences are negative (two major heating terms are positive), vice versa. The question now is as follows: what are the processes that drive the vertical and horizontal wind changes in the MLT region at middle latitudes?

In the following, we first describe the model results at heights from 94 to 600 km (Figures 3 and 7). However, since these parameters in the upper thermosphere and their storm-time changes were much larger than those in the MLT and the changes in neutral parameters in the MLT region are not easy to see in these figures, we plot in Figures 4 and 8 the same parameters in the MLT region from 94 to 110 km with appropriate scales. We also plot in Figures 5 and 6 temperature and wind differences in the upper thermosphere at 405 km (upper panels, a) and in the MLT region at 105 km (lower panels, b). Similarly, we use Figures 7 and 8 to show the changes (storm-quiet time) in meridional and zonal acceleration terms in the thermosphere (94–600 km) and MLT region (94–110 km), respectively.

The top panel in Figure 3a gives meridional winds (V_n) in the storm-time case (storm-time V_n, positive northward) in the Northern Hemisphere at 105°W and 09:40 UT on 17 April 2002, which corresponds to the initial phase of the storm (*Kp* = 6). The storm-time V_n was equatorward above ~150 km from high to low latitudes. The speed of winds was larger than 400 m/s above 220 km at high latitudes. The second panel in Figure 3a gives V_n in the nondisturbed case (nondisturbed V_n). The nondisturbed V_n pattern was similar to the storm-time one, but the speed was smaller than the storm-time one. The bottom panel of Figure 3a shows V_n differences between the top and second panels, which represent the impact of the storm on V_n. V_n differences were equatorward in most of the regions. The upper thermospheric V_n differences were larger and extended more toward the equatorial regions than those below ~220 km. The upper thermospheric V_n differences were greater than 100 m/s at high latitudes from ~75°N to 85°N and over ~300 km but decreased with latitude and became almost zero at ~20°N. Below 150 km around 55°N, V_n differences were equatorward and appeared not directly being connected with upper thermospheric wind changes. Nevertheless,

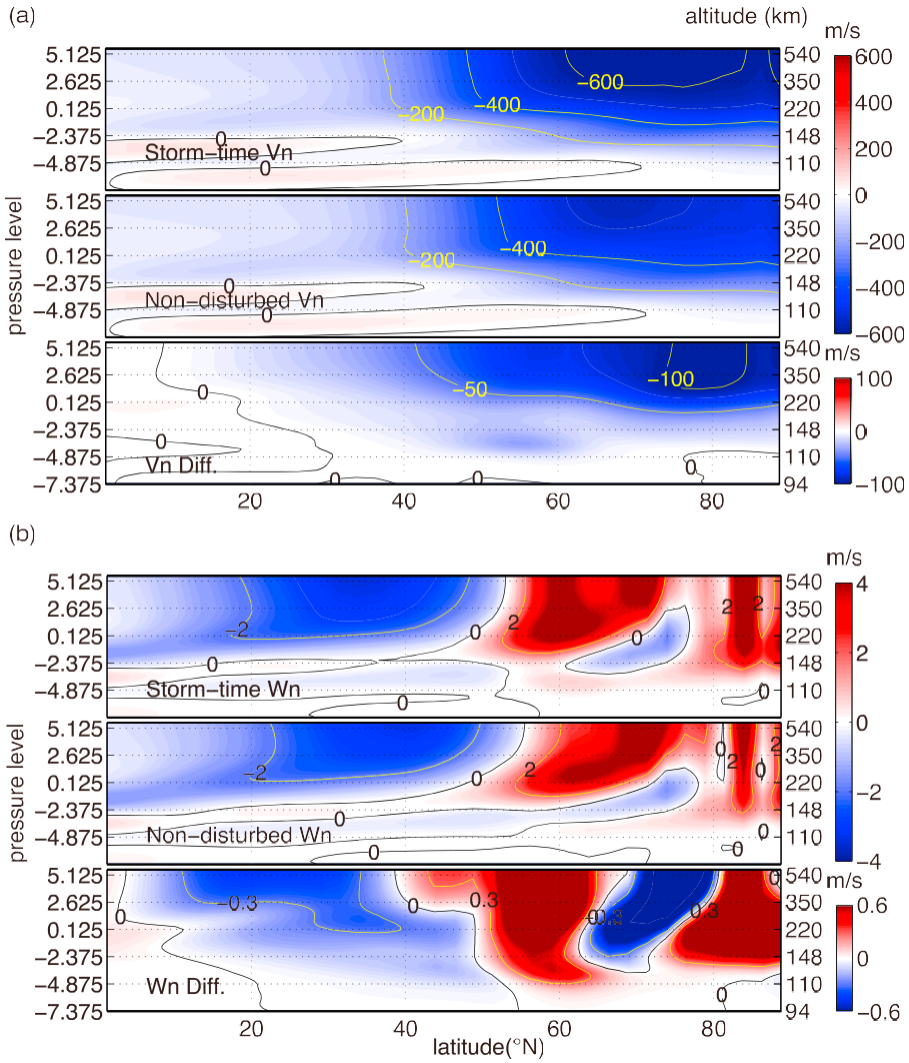

Figure 3. (a, from top to bottom) Latitudinal variations of storm-time meridional winds (positive northward), nondisturbed meridional winds, and their differences at 09:40 UT on 17 April 2002 from 94 to 600 km at 105°W. The black lines represent the zero wind speed. (b) Same as (a), but for the vertical winds (positive upward).

thermospheric circulation at middle latitudes above 150 km was modified in the early phase of the storm, but the lower thermospheric circulation did not change significantly at middle latitudes at that time, as indicated by the zero wind line in the figure.

Figure 3b is the same as Figure 3a, but for the vertical winds (W_n, positive upward). In most of the regions at middle latitudes lower than ~50°N, the storm-time W_n (top panel of Figure 3b) was negative (downward). At high latitudes, W_n was mostly upward. The pattern of the nondisturbed W_n (second panel) was similar to that of the storm-time W_n. The bottom panel shows W_n differences between the top and second panels and represents the storm effects on W_n. W_n differences were negative (downward) at lower latitudes (0–40°N) at almost all heights. W_n differences were also downward between 65°N and 80°N above 150 km but upward in the other regions at higher latitudes. The bottom panel of Figure 3a shows that lower thermospheric V_n did not change at middle latitudes, but lower thermospheric W_n differences changed and were more downward. For instance, V_n differences near 25°N at 150 km were ~0 m/s, but W_n differences at the same location were ~0.02 m/s. During the early phase of the storm, upper thermospheric W_n changes were caused by the divergence/convergence of upper thermospheric horizontal ($\vec{V}_n$) wind changes. The MLT vertical wind changes are the direct effect of those of the upper thermosphere assuming incompressibility. In the MLT region, model results show that there were W_n variations at middle latitudes. However, $\vec{V}_n$ in

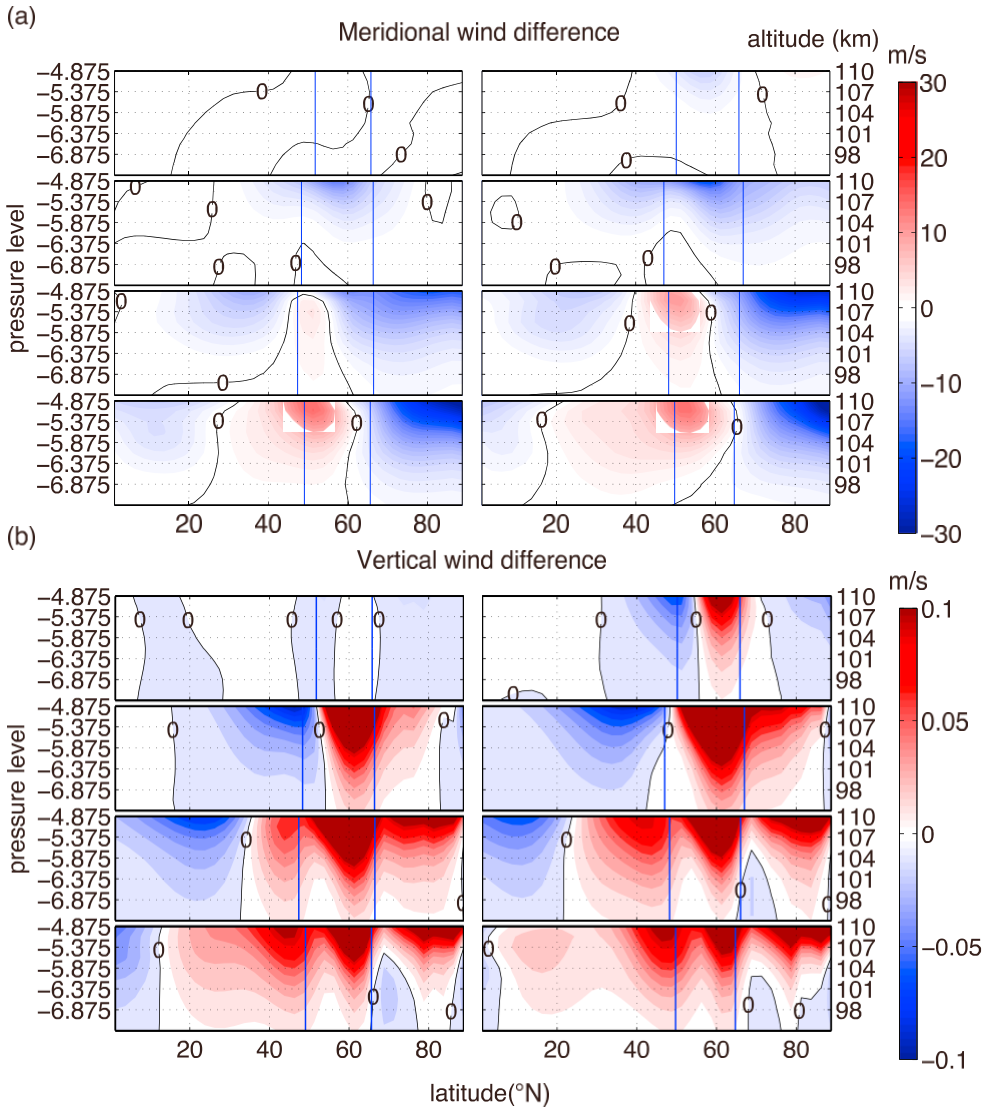

Figure 4. (a, from top to bottom) Latitudinal variations of meridional wind differences (storm − nondisturbed) from 8:00 to 15:00 UT on 17 April 2002 in 1-hr interval from 94 to 110 km at 105°W. The black lines represent the zero wind speed. Two vertical blue lines show the equatorward and poleward boundaries of the auroral oval. (b) Same as (a), but for the vertical winds.

the same MLT region did not change. Therefore, MLT W_n changes at lower latitudes in the early phase of the storm were associated with upper atmospheric W_n changes, not directly the results of local $\vec{V}_n$ changes at the time.

Figure 4 shows the latitudinal variations of meridional winds and vertical wind differences (storm − nondisturbed) in the MLT region at 105°W from 8:00 to 15:00 UT on 17 April 2002. The vertical blue lines give the equatorial and poleward boundaries of the auroral oval. There were small equatorward wind changes inside the auroral oval near 110 km at 09:00 UT in Figure 4a, which were ~10 m/s at 110 km and less than 1 m/s below 104 km. These equatorward (southward) wind changes became larger and expanded toward lower latitudes and polar cap at later UTs. At 12:00 UT, there were two regions of equatorward winds, one in the auroral oval and polar cap and the other in the middle latitudes. The equatorward wind changes in the middle latitudes moved toward lower latitudes with UT and became smaller. Between these two regions, poleward (northward) wind changes occurred around 50°N (inside the auroral oval), then became larger and expanded toward lower latitudes.

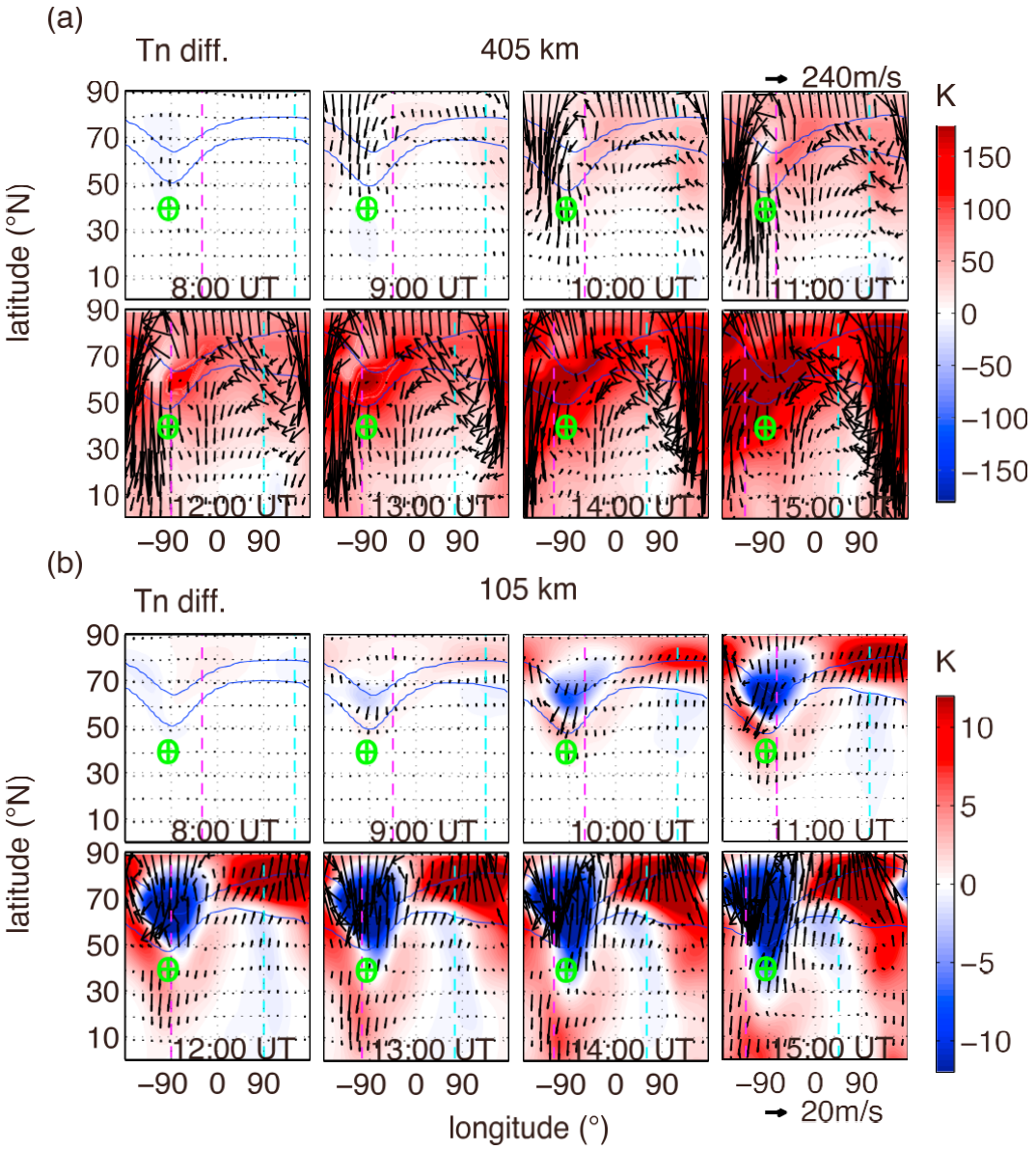

Figure 5. Horizontal wind (vectors) and temperature (color contours) differences (storm − nondisturbed) from 8:00 to 15:00 UT on 17 April 2002 in 1-hr interval at (a) 405 and (b) 105 km. Two blue lines show the equatorward and poleward boundaries of the auroral oval. The pink dashed lines represent 06:00 LT (Local Time), and the blue dashed lines represent 18:00 LT.

Figure 4b shows that large vertical wind changes (>0.1 m/s, as compared to the quiet time vertical wind speed of about 0.3 m/s) are seen in the MLT region at 09:00 UT. One striking feature is that downward vertical wind changes occurred not just inside the auroral oval but also in the middle latitudes from 30° to 55°N, indicating that vertical wind changes occurred earlier than the horizontal wind changes in the middle latitudes. For instance, obvious vertical wind changes of ~0.05 m/s occurred below 104 km, but horizontal wind changes were very small (<1 m/s) at 40°N. Note that the pattern of the small meridional wind changes seen at middle latitudes at 09:00 UT were similar to that at 08:00 UT, indicating that they were not related to storm effects but might be related to the small *Kp* differences between the two runs between 06:00 and 09:00 UT (cf., Figure 1 b). Conversely, the patterns of vertical wind changes were very different between these two UTs.

The region of downward vertical winds expanded and moved toward lower latitudes. It became totally sub-auroral at 11:00 UT. Comparing Figures 4a and 4b, we can see that the peaks of meridional wind changes

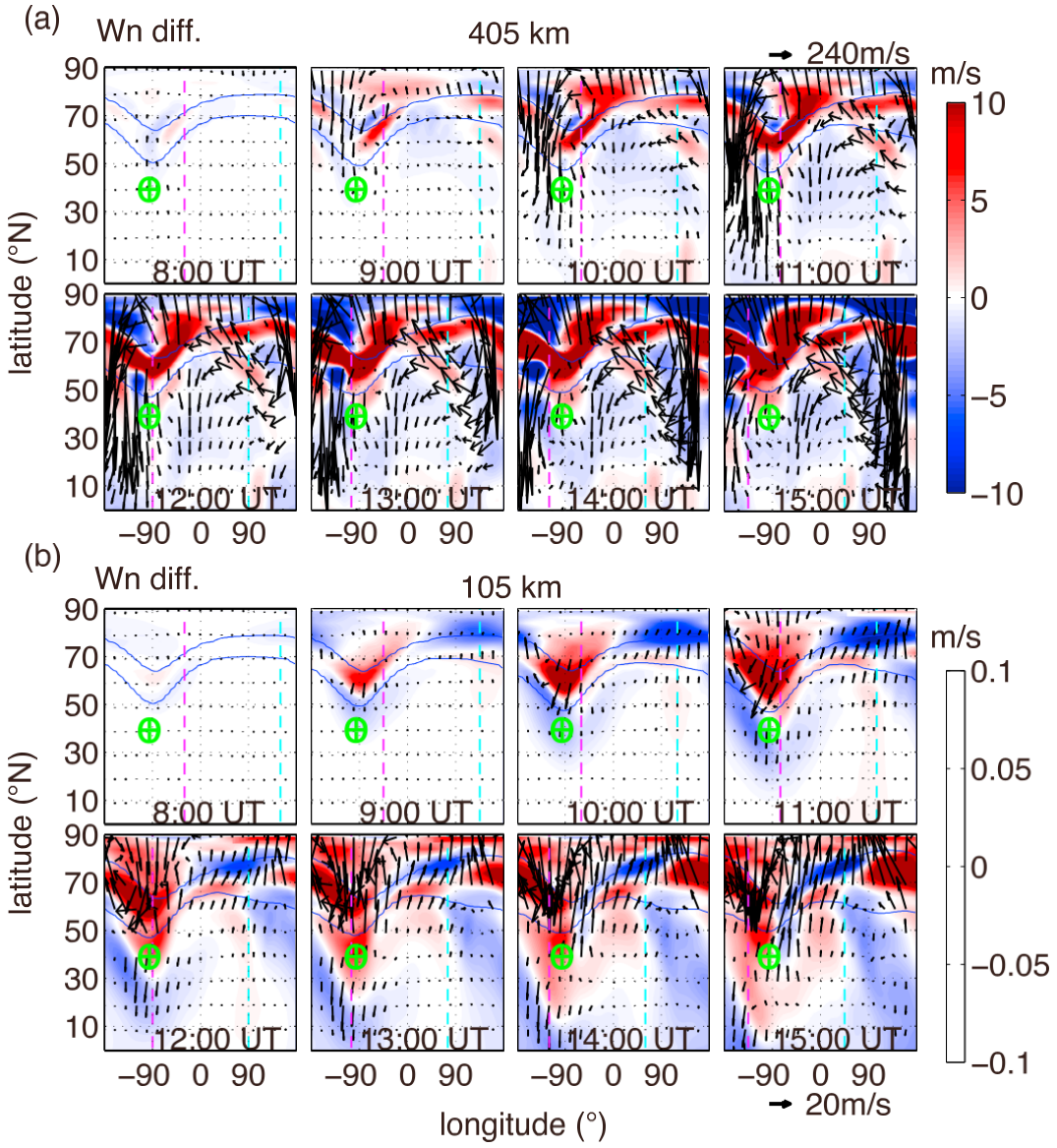

Figure 6. Same as Figure 5, but for vertical wind (color contours) differences.

occurred at higher latitudes than those of the vertical wind changes at the same UT. The peaks of meridional wind changes corresponded roughly to the latitude where vertical wind changes were zero or varied latitudinally from downward to upward.

Another striking feature is that upward vertical wind changes occurred around the auroral oval northward of about 55°N at 09:00 UT. At later UTs, multiple peaks of upward vertical wind changes occurred, including one located inside the auroral oval and one inside the polar cap. Furthermore, there was a broad region of upward vertical wind changes at middle latitudes, which expanded to lower latitudes as the storm progressed.

To illustrate more clearly the storm-time circulation changes at different heights, Figure 5 shows $\vec{V}_n$ and T_n changes (storm − nondisturbed) at two heights: (a) 405 and (b) 105 km. At 405 km, T_n differences (~50 K) can be seen at 09:00 UT (storm onset, 02:00 local time at 105°W) at 50°N and higher latitudes. These changes occurred inside the auroral oval. Two blue lines in the figure show the equatorward and poleward boundaries of the auroral oval. The green circles with crosses give the location of 40°N, 105°W). Conversely, wind differences of ~30 m/s occurred at the latitudes of 45°N and higher near midnight (75°W). T_n and $\vec{V}_n$

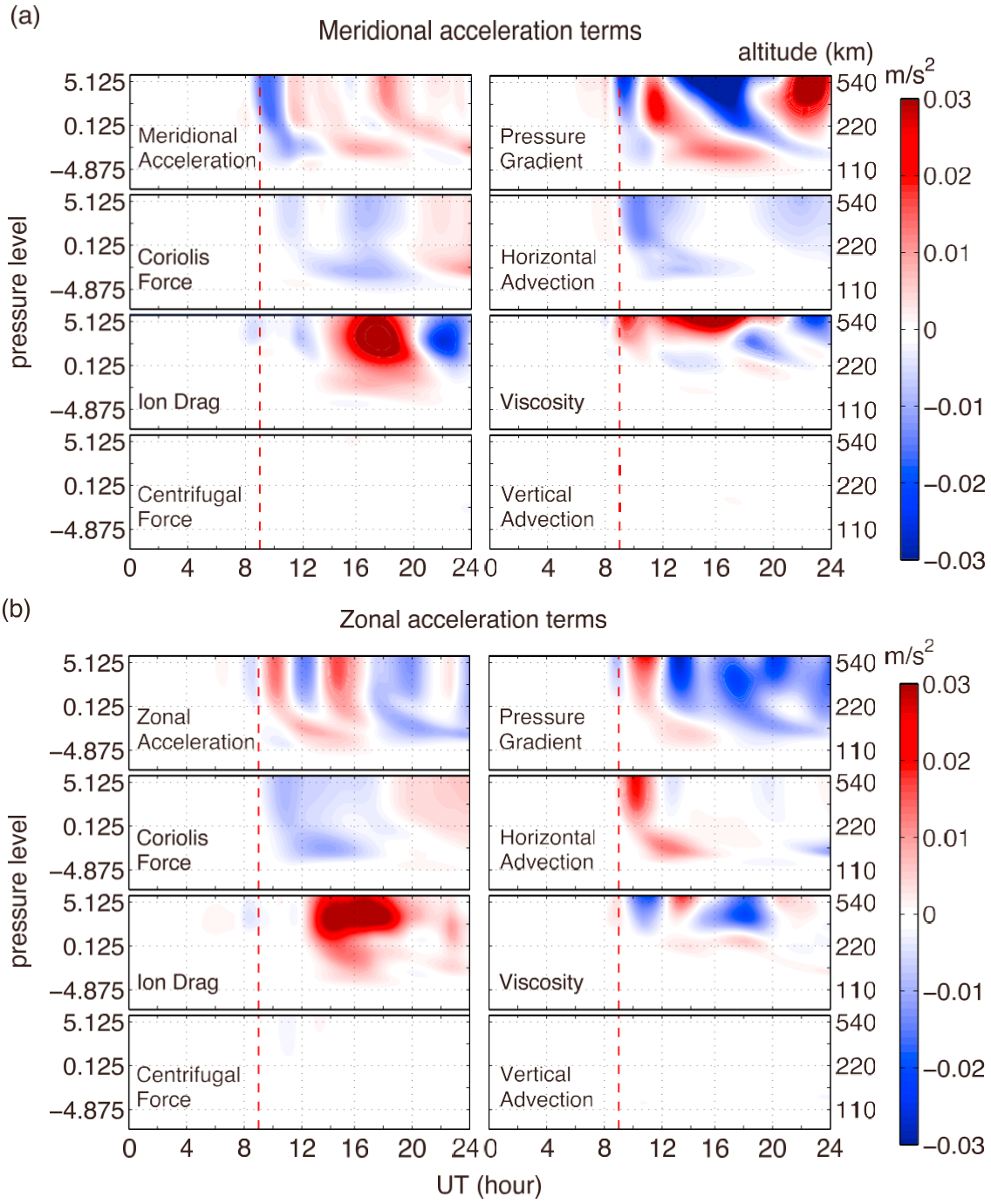

Figure 7. Differences of meridional acceleration terms. (positive northward) From 00:00 to 24:00 UT on 17 April 2002 simulated by the TIMEGCM at the location of 40°N, 105°W from 94 to 600 km. (b) Same as (a), but for zonal acceleration (positive eastward). The red dashed lines indicate the storm onset time.

changes at middle latitudes were small on the dayside (0° to 90°E). T_n and $\vec{V}_n$ at low latitudes were also small for all local times at 09:00 UT. The storm-time variations of daytime T_n and $\vec{V}_n$ also occurred later than those of the nighttime. During most of the storm, the winds were divergent near the auroral oval and convergent at lower latitudes and inside the polar cap in the upper thermosphere.

In the MLT region (Figure 5b), there were no large changes in $\vec{V}_n$ and T_n in most of the Northern Hemisphere at 09:00 UT. However, $\vec{V}_n$ and T_n changes can be seen inside the auroral oval near 90°W,

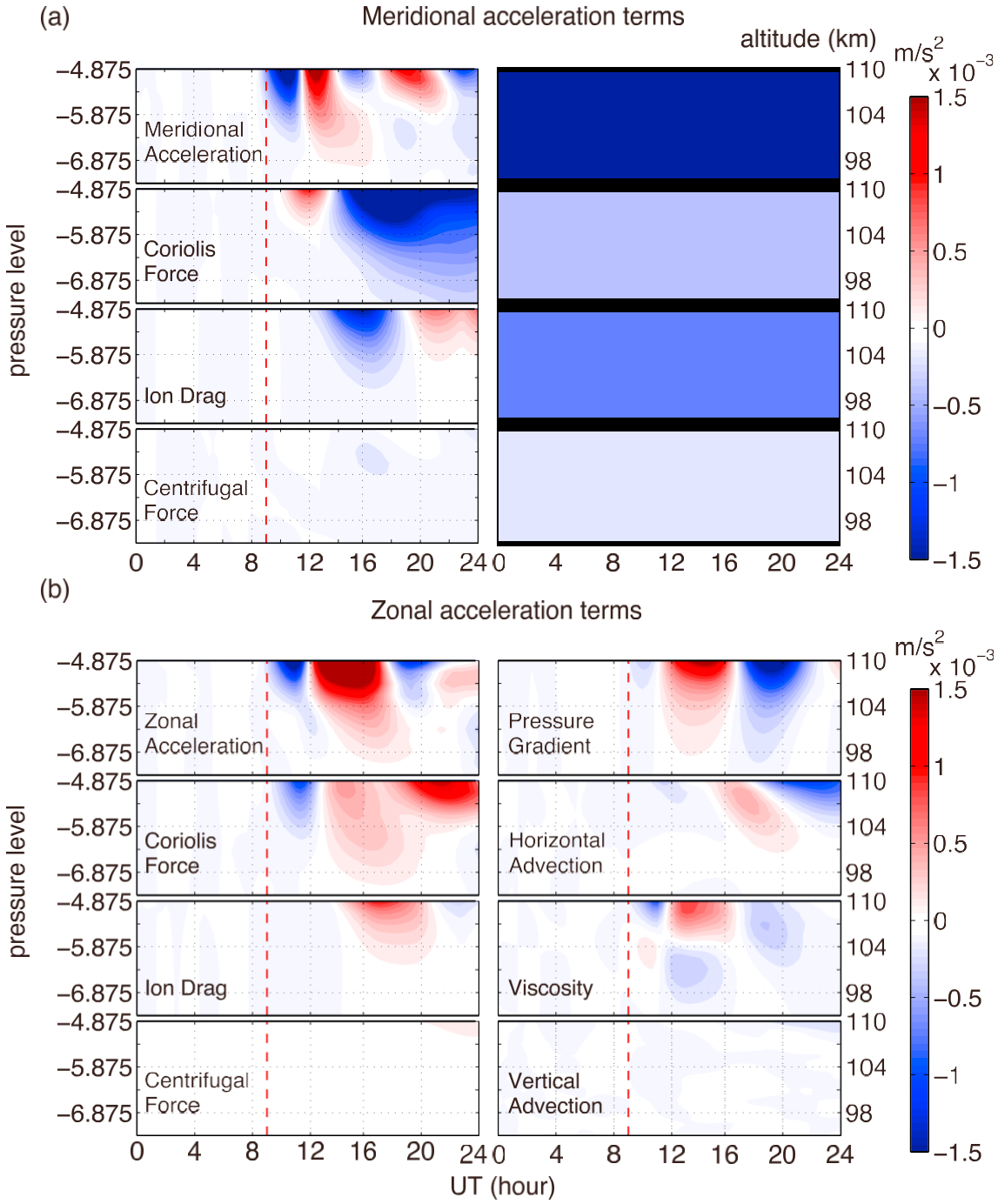

Figure 8. Same as Figure 7, but for the MLT region (94–110 km).

60°N. Small T_n increases can be seen surrounding the region of T_n decrease. This pattern of T_n changes was enhanced and expanded to other longitudes and lower latitudes after 09:00 UT. Before 12:00 UT, V_n differences were equatorward in the middle and high latitudes on the nightside and poleward in the high latitudes on the dayside. The nighttime equatorward wind disturbances in the middle and high latitudes extended to low latitudes as the storm evolved. The daytime poleward wind changes in the high latitudes extended to and were mostly limited to the middle latitudes after 12:00 UT. Similar to the case in the upper thermosphere, T_n and $\vec{V}_n$ changes on the dayside were small at lower latitudes. Note that

equatorward of the auroral oval, MLT $\vec{\nabla}_n$ differences were directed mostly from high temperature regions toward the cold ones.

In Figure 5b, at 12:00 UT and 40°N, there are equatorward V_n differences and eastward U_n differences at 105°W, poleward V_n and westward U_n differences at 90°E, and no obvious changes at 0° longitude. Therefore, the results with a global perspective can explain that observed MLT wind responses to the storms at middle latitudes are still inconclusive, sometimes contradictory in previous studies.

In Figure 6a, upper thermospheric $\vec{\nabla}_n$ and W_n differences changed at 09:00 UT. The storm-time W_n variations on the dayside were smaller than those on the nightside for all UTs. In the MLT region (Figure 6b), the pattern of W_n differences was similar to that of large-scale W_n differences in the upper thermosphere before ~12:00 UT. The equatorward propagation and the pattern of MLT T_n differences were similar to those of MLT W_n differences (cf. Figure 5b). Equatorward of the auroral oval, W_n differences were anticorrelated with T_n changes, and downward W_n corresponded to enhanced T_n. After 12:00 UT, the downward W_n at middle latitudes changed to upward, corresponding to temperature depletion, which is opposite to the situation at earlier times. In the upper thermosphere and near the auroral oval, W_n differences were positive (upward) for all UTs, corresponding to a divergent flow. However, W_n differences in other regions were mostly negative (downward) corresponding to a convergent flow. In the MLT region and in the American sector (nighttime), W_n differences show a bow shape pattern, downward at lower latitudes and upward at higher latitudes. This pattern expanded and extended toward the equator as the storm evolved.

4. Discussion

To understand the mechanisms that cause the storm-time middle-latitude wind changes, Figures 7 and 8 show the changes (storm-quiet time) in acceleration terms (equation (1)). The total acceleration (top left panel in Figures 7 and 8) is the sum of the accelerations by all forcing terms.

In the upper thermosphere, pressure gradient due to temperature changes, horizontal advection, and viscosity (Figure 7) were the dominant forcing terms at middle latitudes (40°N, 105°W, green circles with crosses in Figures 5 and 6) in both the meridional and zonal directions at the beginning of the storm and at night from 10:00 to 11:00 UT. Viscosity was important at very high altitudes, corresponding to the local large gradient in the vertical profiles of the horizontal winds. The total meridional acceleration (forcing) was mostly equatorward in this time period (Figure 7a). The equatorward winds from high latitudes were strong producing equatorward horizontal advection. Because T_n was larger at higher latitudes than at lower latitudes before ~10:00 UT, the acceleration by pressure gradients was also equatorward. After 11:00 UT, upward W_n occurred at the location (Figure 6a). Temperature changes decreased (Figure 5a) due to the adiabatic cooling associated with upward vertical winds. This produced a locally poleward acceleration between 11:00 and 12:00 UT. Thus, local winds are modified mainly due to two processes, one is the high-latitude wind changes that are advected into the middle latitude region, and the other is the wind changes due to pressure gradient changes associated with local T_n changes. When $\vec{\nabla}_n$ changed, W_n were also altered due to changes in the convergence and divergence (Figures 5a and 6a).

The zonal wind acceleration associated with the pressure gradient was eastward from 09:20 to 11:00 UT (Figure 7b) because the T_n variations east of the location were smaller than those west of the location (Figure 5a). After 11:40 UT, the T_n increase in the west of the location began to decrease due to the strong upward vertical winds (Figures 5a and 6a), and the direction of the pressure gradient reversed.

In the upper thermosphere at middle latitudes (Figure 7a), the Coriolis force also contributed to the total changes of acceleration during the storm, but it was relatively small and changed later than the other major forcing terms. Ion drag in the daytime was comparable to the pressure gradient and horizontal advection, both meridional and zonal directions, as was the case between 14:00 UT and 18:00 UT at 40°N, 105°W, when ion drag occurred and was large.

In the MLT region at middle latitudes (Figure 8), the pressure gradient was the dominant forcing term in the meridional direction. Compared to Figure 2, there were downward vertical wind changes at the location of 105°W, 40°N from 09:00 to 11:40 UT, corresponding to increased temperatures (Figure 5b). The pressure gradient associated with local T_n increases caused an equatorward meridional acceleration from the storm

onset until ~11:40 UT. The downward W_n changes extended toward lower latitudes. The temperature changes at low latitudes increased. After ~11:40 UT, W_n at the location became upward, and the MLT region was then experiencing cooling effects. The direction of pressure gradient changed to poleward due to temperature increases in the lower latitudes and so did its associated acceleration. Therefore, V_n changes at the location were equatorward, and increasing with time from 09:00 to 11:40 UT, they then were decelerated and became poleward after ~13:00 UT at 105 km (cf., Figures 5b and 6b). Thus, the peaks of meridional wind changes occurred at roughly the same time as the peaks of temperature changes but relatively later than those of the vertical wind changes. The meridional wind change peaks corresponded roughly to the latitude where vertical wind changes were zero or varied from downward to upward latitudinally (Figure 4).

The zonal acceleration due to the pressure gradient was small before 11:00 UT in the MLT region (Figure 8b). The small pressure gradient was related to the fact that the temperature changes were mostly along the meridional direction. The zonal temperature differences were relatively small. After 11:00 UT, W_n changes caused zonal variations in temperature, and the acceleration due to the pressure gradient turned eastward. The total zonal acceleration was eastward and controlled mainly by the pressure gradient force that was associated with local T_n changes and the Coriolis force. After 17:00 UT, W_n changes became downward and caused temperature increases, and the pressure gradient turned westward. The total zonal acceleration turned westward due to the dominant westward pressure gradient.

During storm time, the Coriolis force was also important for the MLT horizontal wind changes at middle latitudes, but it was reactive to $\vec{V}_n$ changes. Between 09:00 and 13:00 UT and in the meridional direction, the Coriolis force was poleward (Figure 8a) associated with the westward zonal winds. In the zonal direction, the Coriolis force was westward (Figure 8a) caused by the equatorward meridional winds. It then turned to equatorward associated with the eastward winds and eastward related to the northward winds after ~13:00 UT (cf., Li et al., 2018; Figure 2a).

During the storm, ion drag was one of the main drivers of wind changes at high latitudes in the upper thermosphere. However, in the region away from the auroral oval at middle latitudes, ion drag was not strong at night during the storm but has noticeable contribution to the total acceleration during the daytime from 14:00 to 24:00 UT. The large daytime ion drag was due to the large differences between the neutral winds and ion drifts, as well as high plasma densities. However, this is different from the case in the high latitudes. Here the winds were strong, but the ions were confined by magnetic field lines, so the ion drift velocity was relatively small. In this case ion drag is a retarding force, instead of a driving force as it is at high latitudes.

In the MLT region at middle latitudes, horizontal and vertical advection and viscosity are small (Figure 8b). This indicates that MLT wind changes are not the result of momentum transfer from high latitudes or upper thermosphere, as we showed, the wind changes in Region A in Figure 3a were not directly connected with the wind changes at higher altitudes or high latitudes at the same height.

In the upper thermosphere and at high latitudes, when the storm occurs, the enhanced Joule heating and ion drag lead to great changes in neutral temperatures and circulation (e.g., Mayr et al., 1978; McCormac et al., 1987). Note that Joule heating rate per unit volume ($erg \cdot s^{-1} \cdot cm^{-3}$) in the upper thermosphere is smaller than that in the MLT region. The maximum Joule heating rate per unit volume occurs at ~130 km. However, the Joule heating rate per unit mass (K/s) increases with altitude (Jee et al., 2008). Thus, upper thermospheric T_n increase is large due to the large Joule heating rate per unit mass in the upper thermosphere (Huang et al., 2012; Jee et al., 2008). The large T_n changes associated with Joule heating cause strong pressure gradients in the upper thermosphere. The enhanced nighttime meridional winds inside the polar cap are equatorward, and they pass through the auroral oval and blow toward the middle latitudes (e.g., Burns et al., 1991, 1995; Prölss, 2010). Also, the large waves generated by the enhanced Joule heating can quickly propagate to the equator in a few hours after the storm commencement (Figures 3a and 4a; e.g., Burns et al., 1992). As a combined result of horizontal momentum advection from high latitudes, pressure gradient forces caused by temperature change, and the viscous force (Figure 8a), upper thermospheric circulation changes at middle latitudes (Figures 5a and 6a). The large-scale horizontal wind changes result in variations in convergence and divergence, and the circulation changes cause downward vertical winds at lower latitudes and upward vertical winds at higher latitudes (Richmond & Lu, 2000). The strong vertical wind changes lead to adiabatic heating/cooling to the neutral air (Figure 2). The MLT vertical winds vary accordingly with the

upper thermospheric vertical winds. As an example, we pick the location (40°N, 105°W, green circles with crosses in Figures 5 and 6) to show that vertical winds in both the upper thermosphere (405 km) and MLT (105 km) region were downward between 09:00 and 11:40 UT (Figures 2 and 3a). In a recent simulation study, Li et al. (2018) asserted that the TIMEGCM results are similar to and consistent with observations during the simulated storm events. The MLT vertical wind changes are the direct effect of those of the upper thermosphere during the early phase of the storm. This is also evident as both MLT horizontal winds and temperatures (Figures 4a and 5b) had not changed at the time. Downward vertical winds caused adiabatic heating and vertical heat advection; as a result, the MLT temperature at the location (105°W, 40°N) was gradually enhanced (Li et al., 2018), as also shown in Figures 2 and 5b at 10:00 UT. This situation continued until 11:40 UT when the vertical winds changed to upward. This change of the vertical wind direction, however, was the result of local MLT dynamics. The enhanced temperature drove a strong divergent horizontal wind flow and caused upwelling, whereas in the upper thermosphere, vertical wind changes were still downward. The local MLT temperature enhancements then began to decrease in response to changes in MLT vertical winds (i.e., comparing Figure 4b with Figure 5b at 12:00 UT). The winds southward of the location remained equatorward, whereas the winds at higher latitudes changed the direction from equatorward to poleward (cf. Figure 5b 11:00 and 12:00 UT). At later UTs, the local temperature became depleted and connected to the large-temperature depletion region that was extending from high latitudes to middle latitudes. This pattern of wind and temperature changes continued at this location until 15:00 UT when local temperature changes were negative and the wind pattern changed to convergence to make the vertical winds downward again. Note that this pattern expanded and moved toward lower latitudes as the storm evolved. Therefore, storm-time MLT vertical wind changes are more controlled by the changes in the upper thermosphere in the early phase of the storm, but they become more and more dependent on local MLT dynamics as storms progress. Vertical wind changes first cause local temperature increases, which set up a large latitudinal pressure gradient. This gradient then drives a large equatorward meridional circulation (Figure 8b). The local temperature increases become large with time. The resultant pressure gradient then produces a local divergent and upward flow. If the divergent flow is large enough, the MLT vertical wind changes become different from those in the upper thermosphere, for instance, at 13:00 UT. This dynamic process explains the appearance of MLT downward vertical wind at the front edge of the T_n and wind disturbances soon after the storm onset and its expansion toward the lower latitudes (Figure 6b). This also explains the occurrence of upward vertical winds and the expansion of the decreased temperature region from the high latitudes ~3 hr after the storm onset.

In Figure 5b, at 12:00 UT and 40°N, there are equatorward V_n differences and eastward U_n differences at 105°W. The equatorward V_n differences are consistent with the observations of Hook (1970), Ma et al. (2001), and Goncharenko et al. (2004). The storm-time eastward U_n differences also observed by Ma et al. (2001) and Goncharenko et al. (2004). The storm-time MLT poleward wind variations found by Fahrutdinova et al. (2001) can also be seen at 90°W, 50°N from 12:00 to 15:00 UT in Figure 5b. The westward U_n differences at 90°E, 30°N from 12:00 to 14:00 UT in Figure 5b are observed by Singer et al. (1994) and Emmert et al. (2002). Our model results also show no obvious meridional wind changes at (0°, 30°N) from 09:00 to 12:00 UT in Figure 5b, which is consistent with Singer et al. (1994). Therefore, the model results with a global perspective and full temporal variations can explain the observed MLT wind responses to the storms at individual middle latitude sites that may appear inconclusive and sometimes contradictory.

5. Conclusion

In this paper, we examine the effects of geomagnetic storms on MLT winds at middle latitudes. By diagnostically analyzing TIMEGCM outputs during the 17 April 2002 storm, we have reached the following conclusions:

1. In the early phase of the storm, upper thermospheric horizontal wind changes are larger and occur earlier than those in the MLT. They lead to downward changes in vertical winds. The MLT vertical wind changes are also downward and related to the upper thermospheric vertical wind changes. As the storm evolves, the vertical wind changes become more controlled by local MLT dynamics, such as divergence/convergence associated with local temperature changes.

2. The MLT meridional wind changes are equatorward on the nightside. They become larger and extend to low latitudes as the storm progresses. The higher-latitude MLT wind disturbances also turn to poleward. The daytime MLT wind changes are poleward and much smaller than those in the nighttime.
3. The pressure gradient force associated with vertical wind-induced temperature changes and the Coriolis force are the dominant storm-time momentum forcing processes in the MLT at middle latitudes.
4. The momentum transfer from high latitudes or higher altitudes is not the major momentum source for storm-time MLT wind changes at middle latitudes.
5. At middle latitudes, ion drag is small in the MLT region at night. Ion drag contributes to the MLT and upper thermospheric total momentum budget during the daytime when the differences between the velocities of the winds and the ions, as well as ionospheric electron densities, are large.
6. Downward vertical winds increase the MLT temperature, which produces equatorward wind changes in the early phase of the storm. As the storm progresses, the enhanced temperature creates a divergent flow and upward wind changes. These upward winds then lead to a decreased temperature. The wind changes at higher latitudes can then become poleward. This is consistent with the observations that storm-time prevailing meridional winds change direction and speed with time.

Acknowledgments

Simulation data, simulation codes, and analysis routines are being saved on the NCAR High Performance Storage System (https://www2.cisl.ucar.edu/resources/storage-and-file-systems/hpss). The National Center for Atmospheric Research is sponsored by the National Science Foundation (NSF). The *Kp* and *Dst* indexes are obtained from the National Oceanic and Atmospheric Administration website (ftp://ftp.ngdc.noaa.gov/STP/GEOMAGNETIC_DATA). The work is supported by the National Key Research and Development Plan (2018YFC1407305), the National Natural Science Foundation of China (grants 41574158 and U 1631107), the Research Innovation Program for College Graduates of Jiangsu Province (KYCX170897), the Visiting Fellowship from China Scholarship Council (201708320321), and the Natural Science Foundation of Jiangsu Province (BK20140994).

References

Babcock, R. R. Jr., & Evans, J. V. (1979). Effects of geomagnetic disturbances on neutral winds and temperatures in the thermosphere observed over Millstone Hill. *Journal of Geophysical Research*, *84*, 5349–5354. https://doi.org/10.1029/JA084iA09p05349

Burns, A. G., Killeen, T. L., & Roble, R. G. (1991). A theoretical study of thermospheric composition perturbations during an impulsive geomagnetic storm. *Journal of Geophysical Research*, *96*, 14,153–14,167. https://doi.org/10.1029/91JA00678

Burns, A. G., Killeen, T. L., & Roble, R. G. (1992). Thermospheric heating away from the auroral oval during geomagnetic storms. *Canadian Journal of Physics*, *70*, 544–552. https://doi.org/10.1139/p92-089.

Burns, A. G., Killen, T. L., Deng, W., Carignan, G. R., & Roble, R. G. (1995). Geomagnetic storm effects in the low- to middle-latitude upper thermosphere. *Journal of Geophysical Research*, *100*, 14,673–14,691. https://doi.org/10.1029/94JA03232

Emery, B. A., Lathuillere, C., Richards, P. G., Roble, R. G., Buonsanto, M. J., Knipp, D. J., et al. (1999). Time dependent thermospheric neutral response to the 2-11 November 1993 storm period. *Journal of Atmospheric and Solar-Terrestrial Physics*, *61*, 329–350. https://doi.org/10.1016/S1364-6826(98)00137-0

Emmert, J. T., Drob, D. P., Shepherd, G. G., Hernandez, G., Jarvis, M. J., Meriwether, J. W., et al. (2008). DWM07 global empirical model of upper thermospheric storm-induced disturbance winds. *Journal of Geophysical Research*, *113*, A11319. https://doi.org/10.1029/2008JA013541

Emmert, J. T., Fejer, B. G., Fesen, C. G., Shepherd, G. G., & Solheim, B. H. (2001). Climatology of middle- and low-latitude daytime *F* region disturbance neutral winds measured by Wind Imaging Interferometer (WINDII). *Journal of Geophysical Research*, *106*(A11), 24,701–24,712. https://doi.org/10.1029/2000JA000372

Emmert, J. T., Fejer, B. G., Shepherd, G. G., & Solheim, B. H. (2002). Altitude dependence of middle and low-latitude daytime thermospheric disturbance winds measured by WINDII. *Journal of Geophysical Research*, *107*(A12), 1483. https://doi.org/10.1029/2002JA009646

Emmert, J. T., Fejer, B. G., Shepherd, G. G., & Solheim, B. H. (2004). Average nighttime *F* region disturbance neutral winds measured by UARS WINDII: Initial results. *Geophysical Research Letters*, *31*, L22807. https://doi.org/10.1029/2004GL021611

Fahrutdinova, A. N., Sherstyukov, O. N., & Maksyutin, S. V. (2001). Geomagnetic activity influence on the dynamics of the upper mesosphere and lower thermosphere. *International Journal of Geomagnetism and Aeronomy*, *2*, 201–208.

Fesen, C. G. (1997). Geomagnetic activity effects on thermospheric tides: A compendium of theoretical predictions. *Journal of Atmospheric and Solar-Terrestrial Physics*, *59*, 785–803. https://doi.org/10.1016/S1364-6826(96)00106-X

Forbes, J. M., & Roble, R. G. (1990). Thermosphere-ionosphere coupling: An experiment in interactive modeling. *Journal of Geophysical Research*, *95*, 201–208. https://doi.org/10.1029/JA095iA01p00201.

Fuller-Rowell, T. J. (1995). The dynamics of the lower thermosphere. In R. M. Johnson & T. L. Killeen (Eds.), *The upper mesosphere and lower thermosphere: A review of experiment and theory, Geophysical Monograph Series* (Vol. 87, pp. 23–36). Washington, DC.: American Geophysical Union.

Fuller-Rowell, T. J., Millward, G. H., Richmond, A. D., & Codrescu, M. V. (2002). Storm-time changes in the upper atmosphere at low latitudes. *Journal of Atmospheric and Solar-Terrestrial Physics*, *64*, 1383–1391. https://doi.org/10.1016/S1364-6826(02)00101-3

Gardner, L. C., & Schunk, R. W. (2010). Generation of traveling atmospheric disturbances during pulsating geomagnetic storms. *Journal of Geophysical Research*, *115*, A08314. https://doi.org/10.1029/2009JA015129

Goncharenko, L. P., Salah, J. E., Foster, J. C., & Huang, C. (2004). Variations in lower thermosphere dynamics at midlatitudes during intense geomagnetic storms. *Journal of Geophysical Research*, *109*, A04304. https://doi.org/10.1029/2003JA010244

Haaser, R. A., Davidson, R., Heelis, R. A., Earle, G. D., Venkatraman, S. & Klenzing, J. (2013). Storm time meridional wind perturbations in the equatorial upper thermosphere. *Journal of Geophysical Research: Space Physics*, *118*, 2756–2764. https://doi.org/10.1002/jgra.50299

Hagan, M. E., & Forbes, J. M. (2002). Migrating and nonmigrating diurnal tides in the middle and upper atmosphere excited by tropospheric latent heat release. *Journal of Geophysical Research*, *107*(D24), 4757. https://doi.org/10.1029/2001JD001236

Hagan, M. E., & Forbes, J. M. (2003). Migrating and nonmigrating semidiurnal tides in the upper atmosphere excited by tropospheric latent heat release. *Journal of Geophysical Research*, *108*(A2), 1062. https://doi.org/10.1029/2002JA009466

Hagan, M. E., & Sipler, D. P. (1991). Combined incoherent scatter radar and Fabry-Perot interferometer measurements of frictional heating effects over Millstone Hill during March 7–10, 1989. *Journal of Geophysical Research*, *96*, 289–296. https://doi.org/10.1029/90JA02250

Heelis, R. A., Lowell, J. K., & Spiro, R. W. (1982). A model of the high-latitude ionospheric convection pattern. *Journal of Geophysical Research*, *87*, 6339–6345. https://doi.org/10.1029/JA087iA08p06339

Hook, J. L. (1970). Winds at the 75–110 km level at College, Alaska. *Planetary Space Science*, *18*, 1623–1638. https://doi.org/10.1016/0032-0633(70)90037-1

Huang, Y. S., Richmond, A. D., Deng, Y., & Roble, R. (2012). Height distribution of Joule heating and its influence on the thermosphere. *Journal of Geophysical Research*, *117*, A08334. https://doi.org/10.1029/2012JA017885

Jee, G., Burns, A. G., Wang, W., Solomon, S. C., Schunk, R. W., Scherliess, L., et al. (2008). Driving the TING model with GAIM electron densities: Ionospheric effects on the thermosphere. *Journal of Geophysical Research*, *113*, A03305. https://doi.org/10.1029/2007JA012580

Killen, T. L., & Roble, R. G. (1986). Neutral parcel transport in the high latitude F-region. *The Polar Cusp*, *145*, 261–278. https://doi.org/10.1007/978-94-009-5295-9_19

Li, J., Wang, W., Lu, J. Y., Yuan, T., Yue, J., Liu, X., et al. (2018). On the responses of mesosphere and lower thermosphere temperatures to geomagnetic storms at low and middle latitudes. *Geophysical Research Letters*, *45*, 10,128–10,137. https://doi.org/10.1029/2018GL078968

Ma, G., Igarashi, K., & Hocke, K. (2001). Mid-latitude winds in the mesosphere: A superposed epoch analysis over the geomagnetic storm times. *Journal of Atmospheric and Solar-Terrestrial Physics*, *63*, 1993–2001. https://doi.org/10.1016/S1364-6826(01)00064-5

Mayr, H. G., Harris, I., & Spencer, N. W. (1978). Some properties of upper atmosphere dynamics. *Reviews of Geophysics*, *16*, 539–565. https://doi.org/10.1029/RG016i004p00539

Mazaudier, C., & Bernard, R. (1985). Saint-Santin radar observations of lower thermospheric winds. *Journal of Geophysical Research*, *90*, 2885–2895. https://doi.org/10.1029/JA090iA03p02885

McCormac, F. G., Killeen, T. L., Thayer, J. P., Hernandez, G., Tschan, C. R., Ponthieu, J.-J., & Spencer, N. W. (1987). Circulation of the polar thermosphere during geomagnetically quiet and active times as observed by Dynamics Explorer 2. *Journal of Geophysical Research*, *92*, 10,133–10,139. https://doi.org/10.1029/JA092iA09p10133

Nozawa, S., & Brekke, A. (1995). Studies of the *E* region neutral wind in the disturbed auroral ionosphere. *Journal of Geophysical Research*, *100*, 14,717–14,734. https://doi.org/10.1029/95JA00676

Prölss, G. W. (2010). Density perturbations in the upper atmosphere caused by the dissipation of solar wind energy. *Surveys in Geophysics*, *32*(2), 101–195. https://doi.org/10.1007/s10712-010-9104-0

Richmond, A. D., Lathuillere, C., & Vennerstroem, S. (2003). Wind in the high-latitude lower thermosphere: Dependence on the interplanetary magnetic field. *Journal of Geophysical Research*, *108*, 1066. https://doi.org/10.1029/2002JA009493

Richmond, A. D., & Lu, G. (2000). Upper-atmospheric effects of magnetic storms: A brief tutorial. *Journal of Atmospheric and Solar-Terrestrial Physics*, *62*, 1115–1127.

Roble, R. G., & Ridley, E. C. (1994). A thermosphere-ionosphere-mesosphere-electrodynamics general circulation model (TIME-GCM): Equinox solar cycle minimum simulations (30–500 km). *Geophysical Research Letters*, *21*, 417–420. https://doi.org/10.1029/93GL03391

Salah, J. E., & Goncharenko, L. P. (2001). Search for geomagnetic storm effects on lower thermospheric winds at midlatitudes. *Journal of Atmospheric and Solar-Terrestrial Physics*, *63*, 951–963. https://doi.org/10.1016/S1364-6826(00)00192-9

Singer, W., Bremer, J., Hoffmann, P., Manson, A. H., Meek, C. E., Schminder, R., et al. (1994). Geomagnetic influences upon tides-winds from MLT radars. *Journal of Atmospheric and Solar-Terrestrial Physics*, *56*, 1301–1311.

Yuan, T., Zhang, Y., Cai, X., She, S. -Y., & Paxton, L. J. (2015). Impacts of CME-induced geomagnetic storms on the midlatitude mesosphere and lower thermosphere observed by a sodium lidar and TIMED/GUVI. *Geophysical Research Letters*, *42*, 7295–7302. https://doi.org/10.1002/2015GL064860